APL Photonics

Spectral splitting and concentration of broadband light using neural networks

Cite as: APL Photonics **6**, 046101 (2021); https://doi.org/10.1063/5.0042532
Submitted: 31 December 2020 • Accepted: 10 March 2021 • Published Online: 01 April 2021

Alim Yolalmaz and Emre Yüce

Spectral splitting and concentration of broadband light using neural networks

Cite as: APL Photon. 6, 046101 (2021); doi: 10.1063/5.0042532
Submitted: 31 December 2020 • Accepted: 10 March 2021 •
Published Online: 1 April 2021

Alim Yolalmaz[1,2,3] and Emre Yüce[1,2,3,a)]

AFFILIATIONS

[1] Programmable Photonics Group, Department of Physics, Middle East Technical University, 06800 Ankara, Turkey
[2] Micro and Nanotechnology Program, Middle East Technical University, 06800 Ankara, Turkey
[3] The Center for Solar Energy Research and Applications (ODTÜ-GÜNAM), Middle East Technical University, 06800 Ankara, Turkey

[a)] **Author to whom correspondence should be addressed:** eyuce@metu.edu.tr

ABSTRACT

Compact photonic elements that control both the diffraction and interference of light offer superior performance at ultra-compact dimensions. Unlike conventional optical structures, these diffractive optical elements can provide simultaneous control of spectral and spatial profiles of light. However, the inverse design of such a diffractive optical element is time-consuming with current algorithms, and the designs generally lack experimental validation. Here, we develop a neural network model to experimentally design and validate SpliCons; a special type of diffractive optical element that can achieve spectral splitting and simultaneous concentration of broadband light. We use neural networks to exploit nonlinear operations that result from wavefront reconstruction through a phase plate. Our results show that the neural network model yields enhanced spectral splitting performance for phase plates with quantitative assessment compared to phase plates that are optimized via the local search optimization algorithm. The capabilities of the phase plates optimized via the neural network are experimentally validated by comparing the intensity distribution at the output plane. Once the neural networks are trained, we manage to design SpliCons with 96.6% ± 2.3% accuracy within 2 s, which is orders of magnitude faster than iterative search algorithms. We openly share the fast and efficient framework that we develop in order to contribute to the design and implementation of diffractive optical elements that can lead to transformative effects in microscopy, spectroscopy, and solar energy applications.

I. INTRODUCTION

Miniaturized optical elements is an advancing research field aimed to reduce the size, weight, and cost of optical systems while in the meantime enhancing the performance in a variety of application areas such as controlling the phase, polarization[1] and absorption[2] of light beams in a medium that provides superior performance in spectroscopy,[3] sensing,[4] solar energy harvesting,[5] wavelength demultiplexing,[6] particle tracking,[7] imaging,[8] image classification,[9] and quantum computing applications.[10] One of the promising optical elements is phase plates, which provide control over intensity, polarization, and phase distribution of light with a high degree of freedom.[11–15] Their outperforming functionalities are especially required in spectrally splitting broadband light as conventional lenses lack control in the spectral domain.[14–16] However, during the designing of the phase plates, a high number of optimization parameters result in a long computation time that seriously hampers their implementation.[17]

Spectral and spatial dispersion of broadband light finds diverse application areas such as microscopy, digital imaging,[18] projection,[19] and solar energy.[20,21] With the rise in energy demand, intelligent conversion of solar energy is becoming more of a necessity to be addressed fundamentally. The laterally arranged solar cell system has a strong potential in the generation of electricity and incorporates holographic phase plates to achieve spectral splitting of broadband light.[22,23] Unlike conventional diffractive optical elements that are generally designed for one task, SpliCons provide simultaneous spectral splitting and concentration of light.[15] These multi-functional structures can be optimized with iterative approaches. Still, iterative optimization requires immense computational resources and limits the application of SpliCons due to small numbers of controlled parameters that can yield reduced

performance. Instead of iterative approaches, the inverse design of SpliCons can decrease the optimization time. However, the inverse design presents several major challenges compared to the iterative one: (i) phase plates in each frequency of the broadband range are needed, (ii) combination of these phase plates will still require intermediate phase plates to obtain the desired intensity distribution, and (iii) a one-to-many mapping problem.[24] One-to-many mapping is a big problem because a data point may be associated with multiple labels instead of a single class.[25,26] Thus, spectrally splitting and concentrating the light using the inverse design is still an unaddressed challenge. The neural network architecture of deep learning could figure out the one-to-many mapping problem faced in the inverse design of SpliCons and provide fast and accurate control over light beams.

Deep learning is a powerful machine learning technique that can perform time-consuming operations using a multilayered neural network within shorter time scales. This technique has shown great success in various optics and photonics tasks such as microscopy,[27–29] imaging,[30–33] wavelength demultiplexing,[17] metasurface design,[34,35] reconstruction of ultra-short pulses,[36] image classification,[37] beam splitting,[38] and laser-assisted surface machining.[39,40] Moreover, deep learning understands the Fourier transform function by using neural neurons having a single layer with a linear transfer function.[41]

In this study, we develop, for the first time, a neural network model to reconstruct phase patterns for spectrally splitting and spatially concentrating the broadband light and verify our designs experimentally using a spatial light modulator (SLM). In the training procedure of the neural networks, we use a set of known intensity distributions of diffraction patterns and their associated phase plates, where diffraction patterns serve as the input and phase plates that structure light are given as the output. The results indicate our neural network generates phase patterns for spectrally splitting and spatially concentrating light with high accuracy within a few seconds using a single graphics processing unit (GPU). Our network does not require a manual parameter search to optimize the performance of SpliCons and is openly available (see our framework as well as the dataset in the supplementary material) to the community to further accelerate the transformation from uni-functional conventional structures to multi-functional diffraction optical elements.

II. METHODS

A. Experimental setup

The setup for spectral splitting and spatially concentrating the broadband light is presented in Fig. 1(a). The broadband light source from a tungsten–halogen fiber-coupled light source (360–2600 nm, optical power of 7 mW, and optical power noise of 0.3%) first passes through an aspheric condenser lens (f: 16 mm). Next, a linear polarizer adjusts the polarization direction of the light so that it is aligned with the SLM modulation axis. Then, the light is reflected by a mirror and is incident on the SLM (operating between 420 and 1100 nm, Holoeye Pluto-NIR-011 phase-only reflective LCOS, frame rate of 60 Hz). The SLM is placed at a small angle to the transmitted light from the mirror and acts as a pixel-wise phase controller object. The SLM that we use here has pixel dimensions of $8 \times 8\ \mu m^2$ with a total of 1920×1080 pixels. Due to the long optimization duration of a phase plate to concentrate and spectrally split the broadband light, we grouped pixels of the SLM to a matrix size of 64×36 to reduce the number of optimized parameters. Each SLM pixel adds, at maximum, 2.28π phase shift with 0.23π phase steps to the incident light. A phase plate generated by the SLM in the setup controls the phase of the broadband light. The SLM-modulated light passes through a plano–convex lens (f = 200 mm) and is collected by the CCD camera (Allied vision, Guppy Pro F-125; the spectral response of the camera chip is given in Ref. 42). The color-CCD camera pixel dimensions are $3.75 \times 3.75\ \mu m^2$ with a total of 1292×964 pixels. Our experimental setup shows 0.3% noise that includes back-reflections by the equipment, stray light, the light source noise (0.2%), the CCD camera quantification instability, and variation of experiment conditions. In our iterative optimization algorithm, we have targeted the beam of light between 420 and 535 nm (blue band) to the right spot and the light between 560 and 875 nm (red band) to the left spot at the diffraction plane, see Fig. 1.

B. Generation of dataset

While developing a neural network for experimentally spectral splitting and spatially concentrating the broadband light, we generated a dataset using the setup in Fig. 1(a). The data collection procedure is as follows: first, we start with all SLM pixels having zero phase shift. The SLM pixels are grouped by 30×30 forming a superpixel, and totally, 64×36 superpixels exist. The phase of a superpixel is scanned from 0 to 2.28π with a 0.23π phase step. In the meantime, we capture intensity distribution using a color camera. Later, we alter phase shift values of all SLM pixels sequentially and then collect intensity distributions by using a color camera for each phase value of each SLM pixel. In order to perform iterative optimization, we write the phase value on the SLM that gives the highest intensity summation on red and blue target pixels. With this experimental configuration, we obtained 33 796 phase plates [Fig. 1(b)]

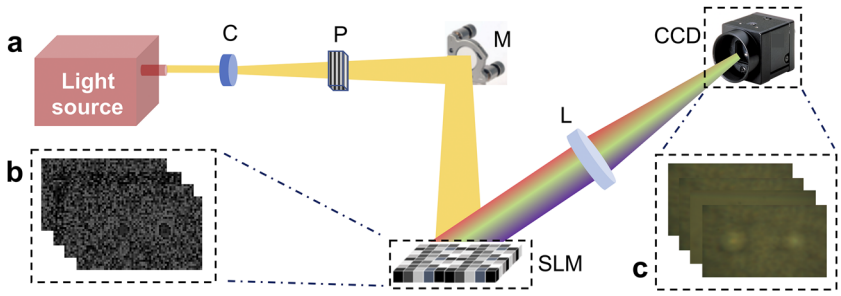

FIG. 1. (a) Schematic of the setup for the spectral splitting and spatially concentrating the broadband light: C, condenser lens; P, linear polarizer; M, mirror (an SLM); L, lens with f = 200 mm; and a CCD camera. (b) Phase patterns that are written on the SLM surface. (c) Intensity distributions measured via the CCD camera.

and corresponding intensity distributions [Fig. 1(c)] formed on the CCD camera. The experimental dataset is collected within 1.7 h that is used for training the neural network only once. After the training, neural network generation of a phase plate for an intensity distribution of interest reduces to 2 s via the neural network. Considering the modeling duration of a neural network, we reduced the SLM pixel size, resulting in a total number of pixels of 36 × 64. In a similar manner, we reduced the size of intensity distributions to a matrix size of 36 × 64. Here, we use percentage differential change (PDC) as a metric to indicate the percentage increase in intensity at the target plane. $PDC^x(\lambda)$ at a pixel position of x for the color band wavelength λ is calculated via Eq. (1). $I_i^x(\lambda)$ and $I_f^x(\lambda)$ are the initial and final intensities at the pixel position of x and color band wavelength λ, respectively,

$$PDC^x(\lambda) = 100 * \frac{I_f^x(\lambda) - I_i^x(\lambda)}{I_i^x(\lambda)}. \quad (1)$$

C. Neural network model

Diffraction of light is expressed by the Fresnel–Kirchhoff diffraction integral, which makes it a suitable problem that can be addressed using convolutional neural network (CNN) layers. The relation between one pixel of the intensity distribution and one pixel of the phase plate depends on many parameters. One pixel of the phase plates has a contribution to each pixel at the target plane.[14] Moreover, when the input wavelength of the phase plate changes, the intensity distribution changes, and there is no explicit pattern between intensity on a target and the input wavelength. Thus, in our neural network model, we employed CNN layers to mimic relations between intensity distributions of formed diffraction patterns and corresponding phase patterns.

The neural network model developed for spectrally splitting and spatially concentrating the broadband light is presented in Fig. 2(a). Using the aforementioned data generation protocol with the experimental setup, we fine-tuned the hyper-parameters and meta-parameters of this model. This model includes 8 CNN layers with a filter size of 9 × 9 and 32 filters. The CNN layers in the model are same-padded for keeping the size of feature maps invariant. After each CNN layer, an activation function of the rectified linear unit (ReLU) is presented to reveal nonlinear relations between the intensity distributions and the phase plates. A ReLU activation function has an output of 0 if the input is less than 0; otherwise, the ReLU activation function gives a raw output. After the fourth CNN layer, down-sampling of the feature maps is performed with a max-pooling operation at each CNN layer. After each max-pooling operation, the number of parameters and computation load in the network is reduced. A fully connected layer with a size of 25 344 and a ReLU activation function are used after flattening operation. Then, we reshaped generated feature maps of the intensity distributions to match the size of the phase patterns. For the classification of the phase values of the phase patterns, we used a softmax activation function. It is a more generalized logistic activation function used in the output layer of a neural network for multi-label classification. Our batch size is selected as 32 for the smooth optimization of model weights. We call the network that we develop Spectral Splitter and Concentrator Network (SpliConNet).

Using the versatile setup that we construct for training and testing SpliCons, we collect 33 796 camera images for training the

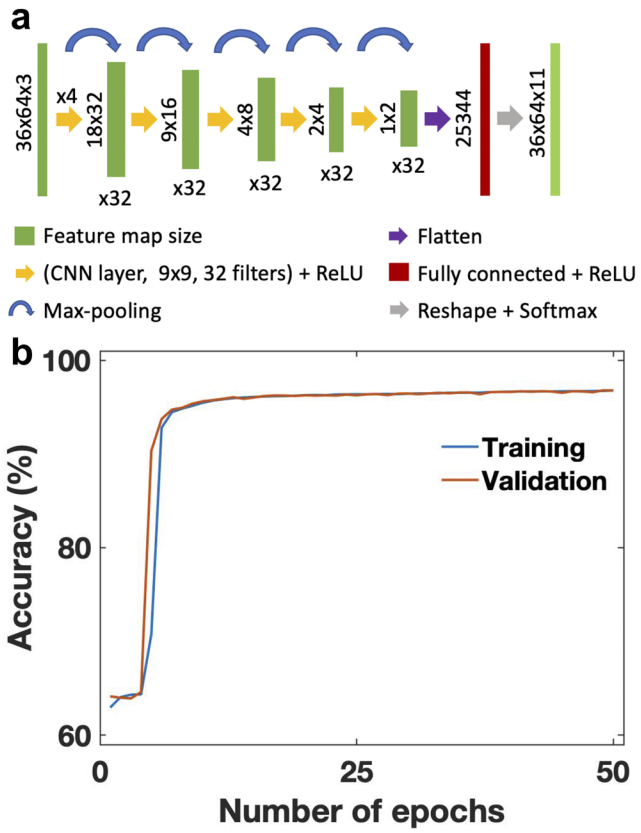

FIG. 2. (a) Neural network model that is trained for experimentally spectral splitting and spatially concentrating the broadband light. (b) Training and validation accuracies of the neural network model with experimental data as a function of epochs, indicating that our model does not result in overfitting.

SpliConNet framework and use normalized intensity distributions in our model. We call Keras and TensorFlow open-source libraries, which provide tools of artificial neural networks in addition to GPU computing operation. We used the ADAM optimizer in TensorFlow to minimize the categorical cross-entropy loss function over the training samples. Training of the model is completed in less than an hour using the TensorFlow library on a NVIDIA Quadro P5000 GPU. The latency of each training epoch is around 5 s. Once the training is completed, we test our model with a validation dataset, which is 10% of the input dataset that is not part of the training set. The validation set prevents overfitting of the network model to the training set [Fig. 2(b)]. After training, it takes only a few seconds to generate a phase plate for the desired intensity distribution.

III. RESULTS AND DISCUSSION

We carried out comprehensive experiments in order to both concentrate and spectrally split the broadband light using a SpliCon and the experimental setup shown in Fig. 1(a). With the setup, we scan pixels of a phase plate to concentrate red and blue bands of the broadband light source on two targets. The phase plate that allows us to disperse the broadband light is presented in Fig. 3(a), and it is

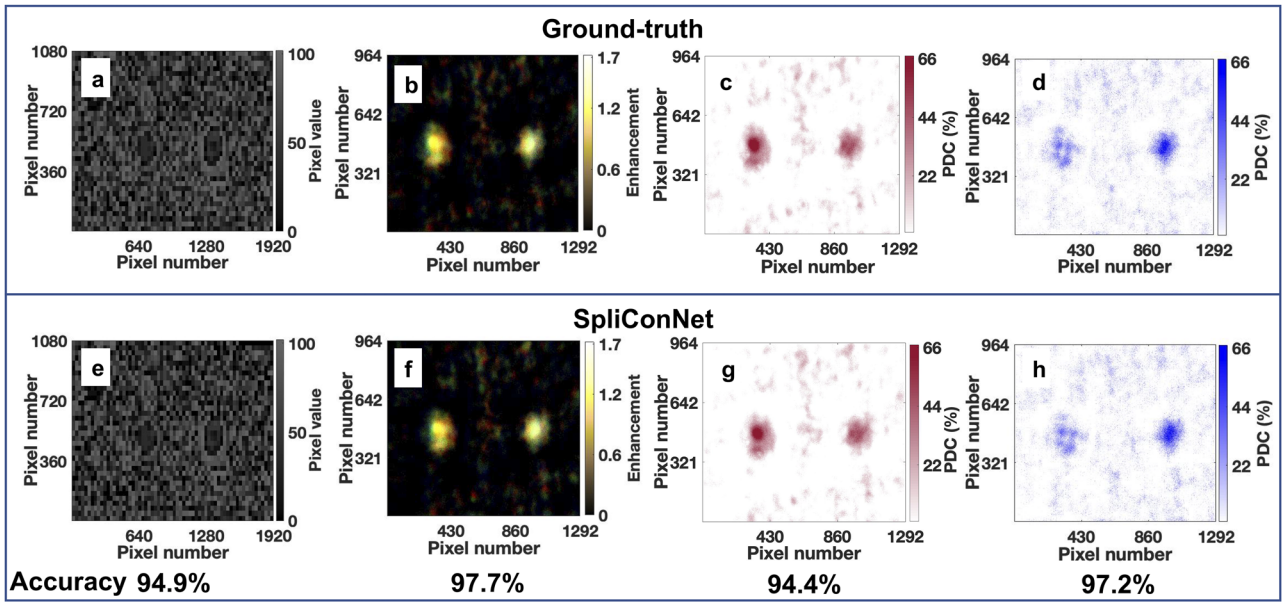

FIG. 3. SpliCon that spectrally splits and concentrates two frequency bands. (a) Iteratively optimized phase pattern to split the broadband light into two bands on two regions. (b) Iteratively obtained intensity distribution of the broadband light on the colorful CCD camera. [(c) and (d)] The intensity distributions of the broadband light for the red channel (between 560 and 875 nm) and blue channel (between 420 and 535 nm). (e) SpliConNet-based phase pattern. (f) SpliConNet-based intensity distribution of the broadband light on the CCD camera. [(g) and (h)] SpliConNet-based intensity distributions of the broadband light channels. Colors of the figures indicate color bands of the broadband light. PDC is the percentage differential increase in intensity described in Eq. (1).

the ground-truth phase plate. Using this ground-truth phase plate, we obtained intensity distribution of the light source, as shown in Fig. 3(b). This image is our ground-truth image to test the neural network model. This procedure is performed only once and takes about 2 h. In Fig. 3(b), we provide the intensity distribution of the broadband light that is split and concentrated into two separate regions. The red band is concentrated on the left of the target plane [Fig. 3(c)] and the blue band is concentrated on the right of the target plane [Fig. 3(d)].

Our goal is to use a neural network model to determine a function of the phase values of the phase pattern, $\phi = f(I, w)$, where I is the intensity of the wavefront shaped light and f is a neural network model parametrized by a set of weights w. With the created data during the optimization of a phase plate, we trained the model in Fig. 2(a). The model includes CNN layers to express function f in terms of weight w. Accuracies of the training and validation through epochs reach around 96.6% ± 2.3% [Fig. 2(b)]. With the results of this figure, we concluded that the weights of the neural network model are well-optimized, and the model lacks over-fitting as we reached similar accuracies with training and validation datasets. We test the performance of our neural network for splitting and concentrating the broadband light. When we reconstruct a phase pattern for the ground-truth CCD image [Fig. 3(b)] by using weights of the neural network, we obtain a similar phase pattern [Fig. 3(e)] with the phase pattern obtained by the experimental study [Fig. 3(a)]. Agreement between these phase plates reaches up to 94.9%, and this value depends on the accuracy of the model, which is affected by the initialization of weights for the model. We saw 97.7% ± 2.7% mean correlation between the reconstructed phase plates with all intensity distributions in the dataset and the ground-truth phase plates.

With the reconstructed phase plate, we obtained a high correlation between the ground-truth CCD image [Fig. 3(b)] and the neural network-based CCD image [Fig. 3(f)], reaching up to 97.7% ± 0.3% accuracy. The result that we obtain is limited by the setup noise of 0.3%. Therefore, the method that we develop succeeds in reaching the ground truth with unprecedented accuracy. With this neural network model, we obtained excess 62.2% enhancement in the red light band [Fig. 3(g)] and 61.0% enhancement in the blue light band [Fig. 3(h)] on the targets, respectively. We observe less than 4.8% error in enhancement values of the light bands with the neural network compared to the experimental results. Considering the experimental setup noise of 0.3%, the error we obtained in the CCD images is well in the expected regime.

In Fig. 4, we present variation of the intensities for two distinct frequency bands. Ground-truth results refer to color bands intensities of the iteratively obtained CCD image. SpliConNet in the same figure corresponds to color bands intensities of the CCD image attained via SpliConNet developed. As shown in Fig. 4, we observe excellent agreement between the ground truth and the SpliConNet optimized intensity patterns.

Neural networks can better understand the fundamental science and drive knowledge discovery in addition to generating useful scientific output using comprehensive datasets. Identifying the input variables that are relevant for estimating the underlying function can assist researchers in better understanding the output of the problem. However, this may not provide information about the underlying physics. We think that physics-informed neural

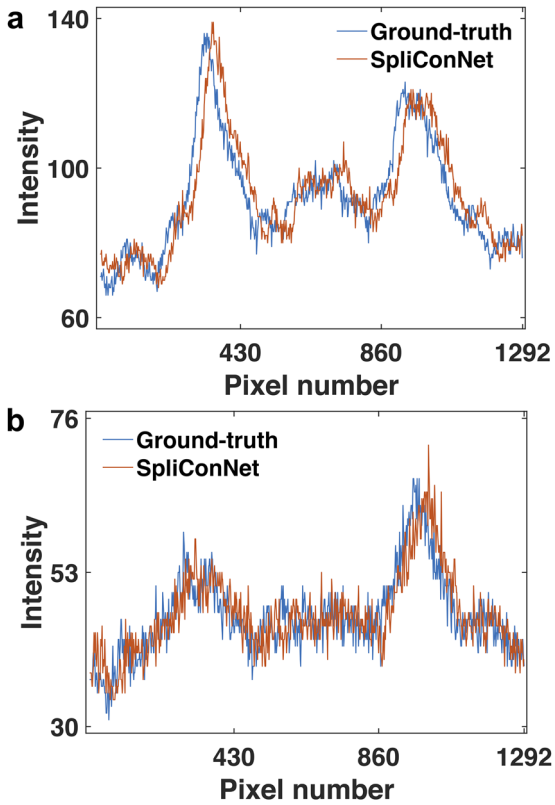

FIG. 4. The output intensity patterns of the SpliCons for (a) red and (b) blue frequency bands that are optimized iteratively (ground-truth) and via SpliConNet. The cross-sectional views are obtained at y = 480 pixel along where color bands are concentrated.

networks can be more beneficial in understanding the underlying physics.[43,44]

Optimizing a phase plate for broadband light is quite a time-consuming process. When the number of optimization parameters, the number of the operating wavelength, the number of pixels, etc. increase, the computation load gets devastated. The number of parameters that we can control here reaches up to 2.50×10^4, and experimental optimization using iterative methods takes up to 2 h. The calculation of a broadband phase plate lasts ~89 days on a desktop PC, which is computationally unaffordable.[14] Our neural network models infer phase patterns from intensity distributions obtained by the Fresnel–Kirchhoff integral without any need for a prior mathematical model of the diffraction within a few seconds. The current approach presented in this manuscript is embodied by using a neural network architecture based on a data-driven approach. Our neural network reveals hidden information between the input and the output data. Thus, spectral and spatial characteristics of broadband light do not affect the phase plate reconstruction capability of our neural network architecture. However, spatial coherence plays a crucial role in shaping the wavefront when a broadband light is used in measurements. The spatial coherence of the sunlight will provide the means to employ our method experimentally.[45]

With the transfer learning tool, we can significantly speed up the training procedure of our neural network model when new dataset is fed from different setup schemes to reconstruct phase patterns for desired intensity distributions. Besides, we can inverse-design phase plates using our neural networks when the size of intensity distribution is up-scaled or down-scaled. Another important feature of our neural network-based spatial light concentration is to control the spot size of modulated light. Further iterative optimization of these phase plate designs yields enhanced efficiencies, and we call this a hybrid technique that constitutes the local search optimization algorithm and the neural network model to improve reconstructed phase patterns of phase plates.

IV. CONCLUSIONS

In this paper, we presented the design of SpliCons using a neural network model. Our model shows high accuracy in reconstructing phase patterns for spectrally splitting and spatially concentrating the broadband light. We obtained 97.7% accuracy in CCD images and 94.9% accuracy in phase plates. Using a reconstructed phase plate, we concentrate more than an excess of 61.0% light on a target. We believe that the spectral and spatial control that we achieve here will pave the way for advanced applications in holography, microscopy, and information technologies in addition to solar energy harvesting. We openly share the fast and accurate framework that we developed in order to contribute to the design and implementation of diffractive optical elements that will lead to transformative effects in diverse fields that require spatial and spectral control of light.

SUPPLEMENTARY MATERIAL

See the supplementary material for the SpliConNet architecture and dataset.

ACKNOWLEDGMENTS

This study was financially supported by the Scientific and Technological Research Council of Turkey (TUBITAK, Grant No. 118F075). The Ph.D. study of Alim Yolalmaz was supported by TUBITAK with the grant program of 2211-A. We thank A. Tarık Temur and M. Ekrem Odabaş for discussions that improved our SpliConNet framework. We thank Alpan Bek and Allard P. Mosk for providing us with the essential equipment.

DATA AVAILABILITY

The data that support the findings of this study are available within the article and its supplementary material.

REFERENCES

[1] A. Arbabi, Y. Horie, M. Bagheri, and A. Faraon, "Dielectric metasurfaces for complete control of phase and polarization with subwavelength spatial resolution and high transmission," Nat. Nanotech. **10**, 937–943 (2015).
[2] D. Sell, J. Yang, S. Doshay, K. Zhang, and J. A. Fan, "Visible light metasurfaces based on single-crystal silicon," ACS Photonics **3**, 1919 (2016).

[3]M. Faraji-Dana, E. Arbabi, A. Arbabi, S. M. Kamali, H. Kwon, and A. Faraon, "Compact folded metasurface spectrometer," Nat. Commun. **9**, 960 (2018).
[4]V. S. Lin, "A porous silicon-based optical interferometric biosensor," Science **278**, 840 (1997).
[5]A. K. Azad, W. J. M. Kort-Kamp, M. Sykora, N. R. Weisse-Bernstein, T. S. Luk, A. J. Taylor, D. A. R. Dalvit, and H.-T. Chen, "Metasurface broadband solar absorber," Sci. Rep. **6**, 20347 (2016).
[6]A. Y. Piggott, J. Lu, K. G. Lagoudakis, J. Petykiewicz, T. M. Babinec, and J. Vučković, "Inverse design and demonstration of a compact and broadband on-chip wavelength demultiplexer," Nat. Photonics **9**, 374 (2015).
[7]A. L. Holsteen, D. Lin, I. Kauvar, G. Wetzstein, and M. L. Brongersma, "A light-field metasurface for high-resolution single-particle tracking," Nano Lett. **19**, 2267–2271 (2019).
[8]N. Borhani, E. Kakkava, C. Moser, and D. Psaltis, "Learning to see through multimode fibers," Optica **5**, 960 (2018).
[9]X. Lin, Y. Rivenson, N. T. Yardimci, M. Veli, Y. Luo, M. Jarrahi, and A. Ozcan, "All-optical machine learning using diffractive deep neural networks," Science **361**, 1004 (2018).
[10]P. Kok, W. J. Munro, K. Nemoto, T. C. Ralph, J. P. Dowling, and G. J. Milburn, "Linear optical quantum computing with photonic qubits," Rev. Mod. Phys. **79**, 135 (2007).
[11]M. Shutova, Z. Liege, A. Goltsov, A. Morozov, and A. V. Sokolov, "Binary phase plate for high-intensity non-diffracting hollow beam structure," J. Opt. Soc. Am. B **36**, 1313 (2019).
[12]H. E. Kondakci, M. Yessenov, M. Meem, D. Reyes, D. Thul, S. R. Fairchild, M. Richardson, R. Menon, and A. F. Abouraddy, "Synthesizing broadband propagation-invariant space-time wave packets using transmissive phase plates," Opt. Express **26**, 13628 (2018).
[13]C. Yang, "Analysis on the focal spot characteristics of random Gauss phase plate," Optik **130**, 601–607 (2017).
[14]A. Yolalmaz and E. Yüce, "Effective bandwidth approach for the spectral splitting of solar spectrum using diffractive optical elements," Opt. Express **28**, 12911 (2020).
[15]B. N. Gün and E. Yüce, "Wavefront shaping assisted design of spectral splitters and solar concentrators," Sci. Rep. **11**, 2825 (2021).
[16]A. Yolalmaz and E. Yüce, "Angle-independent diffractive optical elements for efficient solar energy conversion," Proc. SPIE **11366**, 113660Q (2020).
[17]J. Jiang, D. Sell, S. Hoyer, J. Hickey, J. Yang, and J. A. Fan, "Free-form diffractive metagrating design based on generative adversarial networks," ACS Nano **13**, 8872–8878 (2019).
[18]Y. Zhou, I. I. Kravchenko, H. Wang, J. R. Nolen, G. Gu, and J. Valentine, "Multilayer noninteracting dielectric metasurfaces for multiwavelength metaoptics," Nano Lett. **18**, 7529–7537 (2018).
[19]A. Jesacher, S. Bernet, and M. Ritsch-Marte, "Colour hologram projection with an SLM by exploiting its full phase modulation range," Opt. Express **22**, 20530 (2014).
[20]B. Widyolar, L. Jiang, and R. Winston, "Spectral beam splitting in hybrid PV/T parabolic trough systems for power generation," Appl. Energy **209**, 236 (2018).
[21]A. Elikkottil, M. H. Tahersima, S. Gupta, V. J. Sorger, and B. Pesala, "Silicon nitride grating based planar spectral splitting concentrator for NIR light harvesting," Opt. Express **28**, 21474 (2020).
[22]L. A. A. Bunthof, E. J. Haverkamp, D. van der Woude, G. J. Bauhuis, W. H. M. Corbeek, S. Veelenturf, E. Vlieg, and J. J. Schermer, "Influence of laterally split spectral illumination on multi-junction CPV solar cell performance," Solar Energy **170**, 86 (2018).
[23]C. Stanley, A. Mojiri, M. Rahat, A. Blakers, and G. Rosengarten, "Performance testing of a spectral beam splitting hybrid PVT solar receiver for linear concentrators," Appl. Energy **168**, 303 (2016).
[24]D. Liu, Y. Tan, E. Khoram, and Z. Yu, "Training deep neural networks for the inverse design of nanophotonic structures," ACS Photonics **5**, 1365–1369 (2018).
[25]J. Read, B. Pfahringer, G. Holmes, and E. Frank, "Classifier chains for multi-label classification," Mach. Learn. **85**, 333 (2011).
[26]J. Fürnkranz, E. Hüllermeier, E. Loza Mencía, and K. Brinker, "Multilabel classification via calibrated label ranking," Mach. Learn. **73**, 133 (2008).
[27]Y. Rivenson, Z. Göröcs, H. Günaydin, Y. Zhang, H. Wang, and A. Ozcan, "Deep learning microscopy," Optica **4**, 1437 (2017).
[28]H. Wang, Y. Rivenson, Y. Jin, Z. Wei, R. Gao, H. Günaydın, L. A. Bentolila, C. Kural, and A. Ozcan, "Deep learning enables cross-modality super-resolution in fluorescence microscopy," Nat. Methods **16**, 103 (2018).
[29]Y. Rivenson, H. Ceylan Koydemir, H. Wang, Z. Wei, Z. Ren, H. Günaydın, Y. Zhang, Z. Göröcs, K. Liang, D. Tseng, and A. Ozcan, "Deep learning enhanced mobile-phone microscopy," ACS Photonics **5**, 2354 (2018).
[30]Y. Xue, S. Cheng, Y. Li, and L. Tian, "Reliable deep-learning-based phase imaging with uncertainty quantification," Optica **6**, 618 (2019).
[31]P. Caramazza, O. Moran, R. Murray-Smith, and D. Faccio, "Transmission of natural scene images through a multimode fibre," Nat. Commun. **10**, 2029 (2019).
[32]C. F. Higham, R. Murray-Smith, M. J. Padgett, and M. P. Edgar, "Deep learning for real-time single-pixel video," Sci. Rep. **8**, 2369 (2018).
[33]A. Sinha, J. Lee, S. Li, and G. Barbastathis, "Lensless computational imaging through deep learning," Optica **4**, 1117 (2017).
[34]C. C. Nadell, B. Huang, J. M. Malof, and W. J. Padilla, "Deep learning for accelerated all-dielectric metasurface design," Opt. Express **27**, 27523 (2019).
[35]J. Jiang and J. A. Fan, "Global optimization of dielectric metasurfaces using a physics-driven neural network," Nano Lett. **19**, 5366–5372 (2019).
[36]T. Zahavy, A. Dikopoltsev, D. Moss, G. I. Haham, O. Cohen, S. Mannor, and M. Segev, "Deep learning reconstruction of ultrashort pulses," Optica **5**, 666 (2018).
[37]A. Esteva, B. Kuprel, R. A. Novoa, J. Ko, S. M. Swetter, H. M. Blau, and S. Thrun, "Dermatologist-level classification of skin cancer with deep neural networks," Nature **542**, 115 (2017).
[38]D. Mikhaylov, B. Zhou, T. Kiedrowski, R. Mikut, and A.-F. Lasagni, "High accuracy beam splitting using spatial light modulator combined with machine learning algorithms," Opt. Lasers Eng. **121**, 227 (2019).
[39]B. Mills, D. J. Heath, J. A. Grant-Jacob, and R. W. Eason, "Predictive capabilities for laser machining via a neural network," Opt. Express **26**, 17245 (2018).
[40]D. J. Heath, J. A. Grant-Jacob, Y. Xie, B. S. Mackay, J. A. G. Baker, R. W. Eason, and B. Mills, "Machine learning for 3D simulated visualization of laser machining," Opt. Express **26**, 21574 (2018).
[41]R. Velik, "Discrete Fourier transform computation using neural networks," in *2008 International Conference on Computational Intelligence and Security* (IEEE, 2008).
[42]Guppy Pro Technical Manual, Allied Vis. Technol. GmbH Taschenweg 2a, 07646 Stadtroda/Ger. v4.1.5, 49, 2019.
[43]P. Wiecha, A. Arbouet, C. Girard, and O. Muskens, "Deep learning in nano-photonics: Inverse design and beyond," Photonics Res. (published online, 2021).
[44]M. Raissi, P. Perdikaris, and G. E. Karniadakis, "Physics-informed neural networks: A deep learning framework for solving forward and inverse problems involving nonlinear partial differential equations," J. Comput. Phys. **378**, 686 (2019).
[45]S. Divitt and L. Novotny, "Spatial coherence of sunlight and its implications for light management in photovoltaics," Optica **2**, 95 (2015).